J Mater Sci: Mater Med (2011) 22:1269–1278
DOI 10.1007/s10856-011-4298-3

Evaluation of the biocompatibility of S-phase layers on medical grade austenitic stainless steels

Joseph Buhagiar · Thomas Bell · Rachel Sammons · Hanshan Dong

Received: 13 October 2010 / Accepted: 16 March 2011 / Published online: 25 March 2011

Abstract S-phase surface layers were formed in AISI 316LVM (ASTM F138) and High-N (ASTM F1586) medical grade austenitic stainless steels by plasma surface alloying with nitrogen (at 430°C), carbon (at 500°C) and both carbon and nitrogen (at 430°C). The presence of the S-phase was confirmed by microscopy, hardness testing, depth-profile analysis of chemical composition and X-ray Diffraction. Attachment and proliferation of mouse osteoblast MC3T3-E1 cells were tested on S-phase and untreated controls and the results demonstrated that all the S-phase layers formed were biocompatible under the conditions used. Cells adhered equally well to all samples but proliferation was enhanced on the treated materials.

1 Introduction

AISI 316L austenitic stainless steel is the most popular steel used for orthopaedic implants such as fracture fixation plates and joint replacements. Nevertheless, problems concerning localised corrosion such as pitting and crevice corrosion have been observed with implants of this grade. The development of new steel manufacturing techniques such as vacuum arc remelting has helped to minimise the inclusion content in stainless steel and therefore improved their localised corrosion resistance. For example, vacuum arc remelted 316LVM (ASTM F138) austenitic stainless steel has shown great benefits in a wide range of medical applications. However, it still has limitations with regard to ultimate tensile strength and localised corrosion resistance [1, 2]. Due to this, a new type of high-nitrogen (ASTM F1586) austenitic stainless steel with about 0.4 wt% nitrogen has been developed to improve the corrosion resistance and strength [1–3]. Both ASTM F138 and F1586 show good tissue acceptance and fulfil the requirements of the current standards for surgical implants and the latter has been successfully used in Europe as a material for cemented hip prosthesis [1].

The low hardness and poor wear resistance of these austenitic stainless steels are however their major limitations for tribological applications (such as joint bearing surfaces) [4]. In 1985 Zhang and Bell [5] developed a low temperature plasma nitriding treatment that can increase the hardness and wear resistance of austenitic stainless steels without any detriment to their corrosion resistance. This was achieved by creating a nitrogen-supersaturated modified layer, termed the S-phase or expanded austenite. Since then, low temperature surface alloying with N (nitriding) [6], C (carburising) [7] and both N and C (carbonitriding) [8] have produced promising improvements in combined hardness, wear resistance and corrosion resistance of nitrogen S-phase (S_N), carbon S-phase (S_C) and nitrogen/carbon S-phase (S_{C-N}) layers respectively.

Independent studies [9–14] have confirmed that S-phase surface engineering of ASTM F138 and ASTM F1586

No benefit of any kind will be received either directly or indirectly by the authors.

J. Buhagiar (✉) · T. Bell · H. Dong
School of Metallurgy and Materials, The University of Birmingham, Birmingham B15 2TT, UK
e-mail: joseph.p.buhagiar@um.edu.mt

R. Sammons
School of Dentistry, The University of Birmingham, Birmingham B4 6NN, UK

Present Address:
J. Buhagiar
Department of Metallurgy and Materials Engineering, University of Malta, Msida, MSD 2080, Malta

results in an improvement of the hardness and wear properties without any detriment to the corrosion resistance but no work has been done to evaluate their biocompatibility except for two studies on low temperature nitrided AISI 316L stainless steel by Bordji et al. [15] and Martinesi et al. [16]. However it is not clear if S_N had been formed in the work of Bordji et al. [15] since no reference was made to the S-phase. Therefore, it is essential to evaluate the biocompatibility of S-phase surfaces, to lay a foundation for potential biomedical applications.

This paper reports the preparation and characterization of nitrogen S-phase (S_N), carbon S-phase (S_C) and nitrogen/carbon S-phase (S_{C-N}) layers formed on ASTM F138 and F1586 by low temperature plasma surface alloying with N, C and both N and C. Biocompatibility of the layers was then evaluated using the mouse osteoblast cell line MCT3T3-E1 to monitor cell proliferation, viability, morphology and spreading on the different surfaces.

2 Materials and methods

2.1 Materials

The compositions of ASTM F138 (Sandvik Bioline 316LVM) and ASTM F1586 (Sandvik Bioline High-N) austenitic stainless steels used in this study are shown in Table 1. The material was acquired in a 14 mm diameter bar form and both bars were supplied in the cold worked condition.

Coupon samples of 6 mm thickness were cut from the 14 mm cold worked bars and one of the flat surfaces was then wet ground using silicon carbide paper from 120 down to 1200 grit. Prior to plasma surface alloying treatments samples were ultrasonically cleaned in acetone and dried with hot air, as previously described [12, 13, 17].

2.2 Treatments

The two types of stainless steel were subjected to three different low temperature plasma surface alloying treatments: (1) with N (plasma nitriding; PN); (2) with C (plasma carburising; PC) and (3) with both N and C (plasma carbonitriding; PNC).

Surface treatment conditions were selected to form precipitate free S-phase layers [12, 17] and sample codes are given in Table 2. Following the surface treatment, all treated and untreated samples were polished to a similar surface finish (Ra) between 0.09 and 0.12 μm and then cut again so that the sample thickness was reduced to 1 mm.

2.3 Optical microscopy

Metallographic specimens were prepared using standard procedures and examined with a Leitz DMRX optical microscope. Cross-sections were prepared normal to the surface, mounted in phenolic resin, wet ground with silicon carbide paper from 240 down to 1200 and polished with diamond water based suspensions of 6, 1 and ¼ μm size in sequence. After polishing, the samples were cleaned in acetone and etched for 5 s in a solution containing 50 ml HCl (39% conc.), 25 ml of HNO_3 (69% conc.) and 25 ml of distilled water.

2.4 Hardness and surface topography measurements

Surface hardness was measured using a Mitutoyo MVK-H1 micro-hardness tester with a Vickers indenter at a range of loads between 0.05 to 0.10 kgf with five repeats for each measurement.

A Laser Confocal Microscope, Olympus Lext OLS-3100, was used to measure surface roughness. Three points on each sample were measured and the average Ra values reported.

2.5 Chemical analysis and contact angle measurements

Chemical composition depth-profile analysis was carried out using a LECO GDS-750 QDP glow discharge optical emission spectroscopy (GDOES). This equipment was calibrated for all the alloying elements with special attention to N and C. Carbon was calibrated using cast iron and stainless steel standards for the high and low end of the calibration curve. Elemental N was similarly calibrated with a Coronite® standard and stainless steel standards. The depth was also determined using a profilometer and found to agree with the computed depth.

Contact angles were measured using a KRÜSS GmbH EASYDROP Contact Angle Measuring System by the

Table 1 Composition of the two materials

Material	Composition (wt%)											
	C	Si	Mn	P	S	Cr	Ni	Mo	Cu	N	Nb	Fe
ASTM F138	0.021	0.49	1.68	0.018	0.001	17.43	14.22	2.77	0.082	0.055	–	Bal.
ASTM F1586	0.032	0.48	4.05	0.016	0.0008	20.70	9.70	2.33	0.1	0.38	0.26	Bal.

Table 2 Process Parameters for LTPSA treatments

Material	Code	Process parameters					
		Temperature	Time	Pressure	Gas mix [%]		
		(°C)	(h)	(mbar)	CH_4	N_2	H_2
ASTM F138	MN430	430	15	4	0	25	75
ASTM F138	MNC430	430	15	4	1.5	25	73.5
ASTM F138	MC500	500	15	4	1.5	0	98.5
ASTM F1586	NN430	430	15	4	0	25	75
ASTM F1586	NNC430	430	15	4	1.5	25	73.5
ASTM F1586	NC500	500	15	4	1.5	0	98.5

sessile drop method under distilled water. The tests were performed at ambient humidity and temperature and 3 drop measurement were taken on each specimen to yield a statistical average.

2.6 X-radiation diffraction (XRD)

The phase constituents in the as-received and plasma treated surfaces were analysed with an X'Pert Philips X-Radiation diffractometer using Cu-Kα radiation ($\lambda = 0.154$ nm). The scanning step was 0.02° at a dwelling time of 3 s. The diffraction patterns obtained were analysed and indexed using X'Pert High Score analytical software for automated powder diffraction.

2.7 Biocompatibility evaluation

2.7.1 Preparation of cell suspensions

MCT3T3 (American Type Culture Collection™) E1 mouse osteoblast cells were cultured in 200 ml of McCoy's 5A Medium containing L-Glutamine (Gibco™) to which was added 20 ml of Fetal Calf Serum (Sigma™); 5 ml HEPES (Sigma™); and 2 ml of Penicillin/Streptomycin (50 units ml^{-1} Sigma™). Cultures were incubated in 5% (v/v) carbon dioxide at 37°C. Cells were harvested using 0.25% trypsin–EDTA (Sigma™) and suspensions containing 100,000 cells ml^{-1} and 25,000 cells ml^{-1} were used for the viability assays and the cell attachment assays respectively.

2.7.2 Cell proliferation assays (MTT Test)

The metallic discs (14 mm diameter; 1 mm thickness) and control plastic samples (13 mm Thermanox® coverslips) were placed in the (15 mm diameter) wells of 24-well plates (Costar®). Three samples of each type were used for each time point with an additional sample for SEM (JEOL 7000). A cell suspension containing 1×10^5 cells ml^{-1} was prepared and 1 mL of this was added per well, to a depth of approximately 2 mm above the surface of the samples. Cultures were incubated in 5% (v/v) carbon dioxide (CO_2) at 37°C for 1, 2 and 3 days.

Cell numbers were compared by an MTT test, which is based on the reduction of tetrazolium salt to formazan. This reduction is affected by both changes in cell number and cell metabolism. 60 µl of MTT (3-(4,5-dimethylthiazol-2-yl)-2,5-diphenyltetrazolium bromide); 5 mg/ml; (Sigma™) solution in PBS were added to the wells containing samples to be assayed. The plates were placed on a shaking table for 5 min and then incubated for four hours in 5% (v/v) carbon dioxide (CO_2) at 37°C in order for the cells to metabolize the MTT. Each metallic disc or Thermanox coverslip control was then transferred into a new 24-well plate (in order to assay only the cells growing on the samples) and 1 ml of fresh medium per well was added followed by 400 µl of dimethylsulphoxide (Sigma™) to solubilise the formazan. Five minutes after the removal of the samples, an Elisa (ELX300) plate reader was used to read the absorbance at a wavelength of 570 nm. Absorbance readings were converted to cell number by reference to a calibration curve.

2.7.3 Cell attachment assays

Cells were allowed to recover from the trypsin harvesting treatment for 30 min in an incubator at 37°C prior to use (to minimise the effect of trypsin damage to integrins). Three metal samples per condition were exposed to approximately 500,000 cells in 20 ml of media for 30 min at 37°C in 5% (v/v) CO_2. The cell suspension was then discarded and the samples were rinsed with PBS to remove any unattached cells. Samples were then fixed, and prepared for SEM.

The number of cells attached to implant surfaces was determined from 3 replicate experiments (3 samples per condition) in an area of 0.03 mm^2. Cells were classified according to 4 stages of attachment as described by Rajaraman et al. [18]. In this classification, the first stage is characterized by rounded cells with a few filopodia, which

progress to cells with focal cytoplasmic extensions or lamellipodia (stage 2), circumferential spreading (stage 3), and full spreading and flattening into a polygonal shape (stage 4).

3 Results

3.1 Materials characterisation

Figure 1 shows representative micrographs of the S-phase layers formed in ASTM F138 (Fig. 1 a, c, e) and ASTM F1586 (Fig. 1 b, d, f) austenitic stainless steel after plasma alloying with N at 430°C, N and C at 430°C and C at 500°C.

All the S-phase layers formed appear to be bright and featureless. This implies that when compared to the substrate, the layers formed during low temperature surface alloying are probably precipitation free with superior corrosion resistance to the attack of the etchant used.

Figure 2a displays the XRD plots of the three treated ASTM F138 samples together with that of the untreated material. In comparison with the untreated material there is a shift in peaks to lower angles and broadening of the peaks. This is the characteristic signature of the S-phase layer. The angle shift and broadening is highest for the nitrided samples, followed by carbonitrided and carburised samples. X-ray Diffraction analysis of the treated ASTM F138 samples shows that the layers created in this alloy are composed of S-phase without any precipitates.

By contrast, XRD analysis of the treated ASTM F1586 High-N alloy, Fig. 2b, shows that the layers are composed mainly of the S-phase together with some iron carbides (Fe_3C). The identified carbides reside only at the very surface since they disappeared after polishing away less than 1 μm of the surface layer.

Because of the cementite (Fe_3C) XRD peaks, that are due to a deposited layer close to the surface, it was decided to polish off the first 1 μm of the layer to ensure that we were only testing the biocompatibility of the S-Phase layer. The polishing also ensured parity of surface finish of treated and untreated samples.

The depth distributions of nitrogen and carbon can be seen in Fig. 3. The thickness of the nitrogen- and carbon-diffused layers as determined from the nitrogen and carbon depth profiles is in good agreement with those measured from the optical microscope cross-section microstructures shown in Fig. 1.

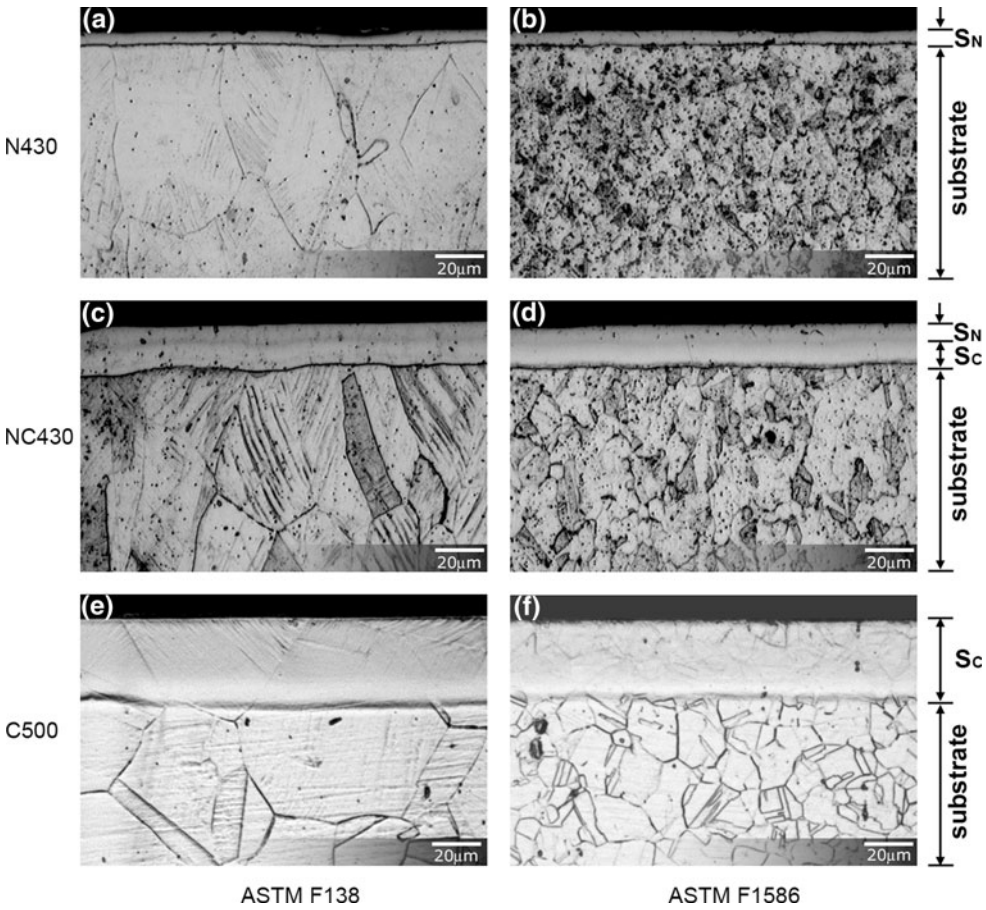

Fig. 1 Cross-sectional microstructure of S-phase layer formed in ASTM F138 (**a**, **c**, **e**) and ASTM F1586 (**b**, **d**, **f**) austenitic stainless steel after: **a**, **b** PN at 430°C [MN430 and NN430]; **c**, **d** PNC at 430°C [MNC430 and NNC430]; and **e**, **f** PC at 500°C [MC500 and NC500]

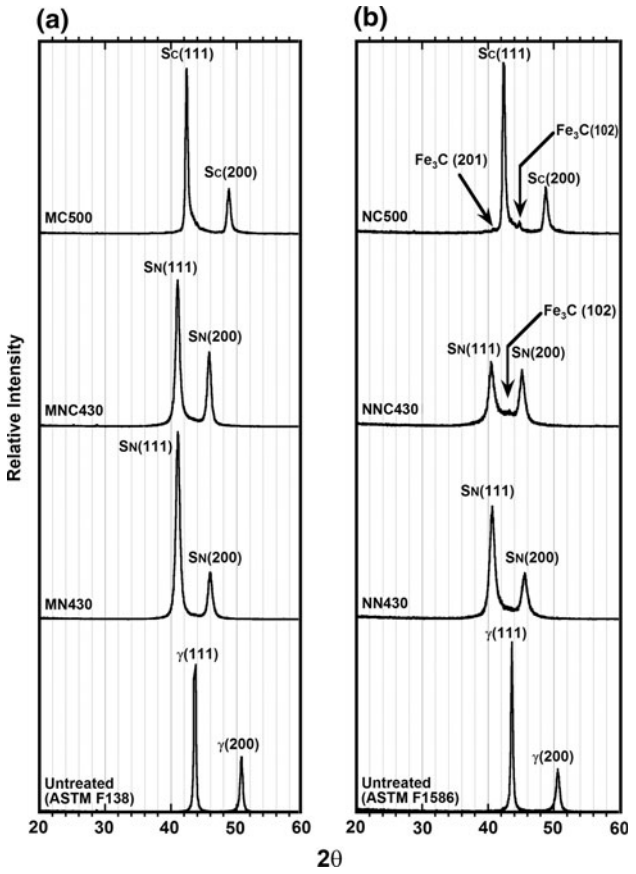

Fig. 2 XRD patterns of untreated **a** ASTM F138 and **b** ASTM F1586 austenitic stainless steel compared to modified layers formed after: PN at 430°C (MN430 and NN430); PNC at 430°C (MNC430 and NNC430); and PC at 500°C (MC500 and NC500)

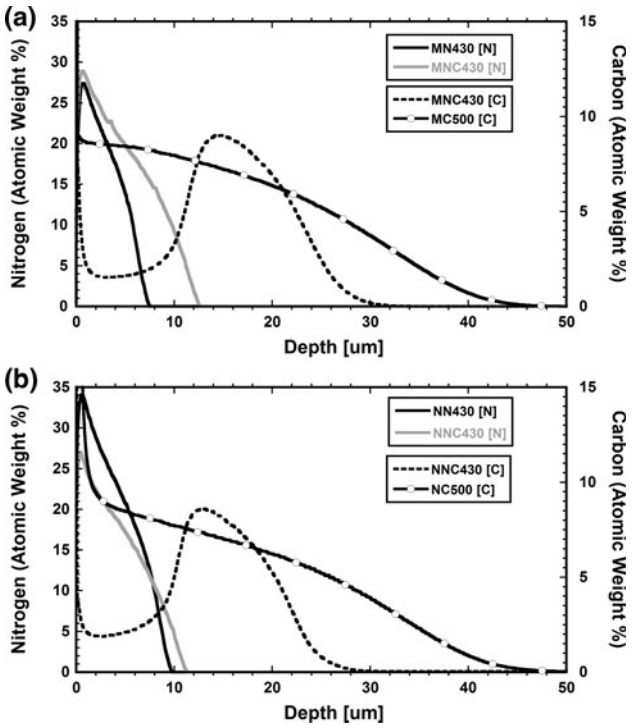

Fig. 3 Composition-depth profiling of **a** ASTM F138 and **b** ASTM F1586 austenitic stainless steel modified layers formed after: PN at 430°C (MN430 and NN430); PNC at 430°C (MNC430 and NNC430); and PC at 500°C (MC500 and NC500)

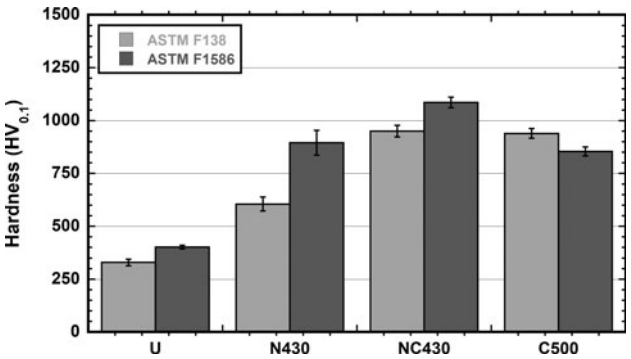

Fig. 4 Hardness of ASTM F138 and ASTM F1586 in the untreated (U), nitrided at 430°C (N430), carbonitrided at 430°C (NC430) and carburised at 500°C

For both treated materials, the 430°C nitrided layer was about 10 μm thick with a surface nitrogen content of 30–35 at.% and the thickness of the 500°C carburised layers was 45 μm. The analysis of the carbonitrided layers indicated that the S-phase layer formed was divided into two sublayers: a top nitrogen-rich (~25 at.%) sublayer followed by a carbon-rich (8 at.%) sublayer. The thicknesses of the nitrogen-rich sublayer and the total layer were approximately 10 and 26–28 μm, respectively.

Figure 4 summarises the hardness results for treated ASTM F138 and ASTM F1586. It can be clearly seen that both alloys can be hardened significantly using any of these surface alloying processes. Both materials exhibited very similar hardening effects and the surface hardness decreased in the order: carbonitrided > carburised > nitrided > untreated.

3.2 Biocompatibility and cell proliferation

Figure 5 represents the number of viable osteoblasts after 1–2 days on ASTM F138 and ASTM F1586, determined by the MTT test. Because the number of replicates was very small the differences observed were not significant and further experiments will be carried out to determine the effects of the different treatments. Representative images for ASTM F138 and ASTM F1586 after 1 and 3 days are shown in Fig. 6. All the samples permitted cell attachment and proliferation and higher metabolic activity, corresponding to more cells on the treated samples in comparison with the controls after 1 and 2 days. At later time periods the differences were less pronounced as the cells became confluent and metabolic activity slowed down.

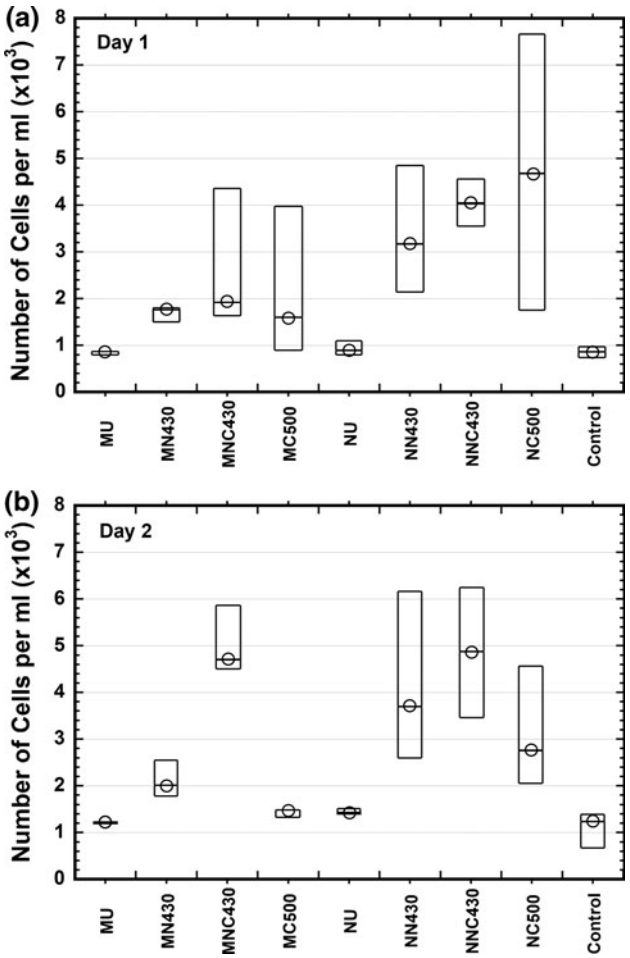

Fig. 5 Osteoblast proliferation kinetics on Thermanox (control), ASTM F138 (treated and untreated) and ASTM F1586 (treated and untreated) after **a** 1 day and **b** 2 days of culture

Differences between the treated surfaces were most pronounced after 2 days when significantly higher activity was seen on the nitrocarburised samples in comparison with the others and the controls. This pattern was seen with both ASTM F138 and F1586. The SEM images confirmed the increased number of cells on the nitrocarburised samples on both materials. There was no evidence of changes in cell morphology or cell damage.

3.3 Cell attachment

The differences in numbers of proliferating cells on the different surfaces could be due to higher initial cell attachment, or a higher rate of spreading or proliferation. Figures 7 and 8 show that similar numbers of cells had attached to ASTM F138 and ASTM F1586 respectively after 30 min.

This was confirmed by counting the total number of cells in an area of 0.03 mm^2 in the SEM images of three different samples and determining the average (Fig. 9a). There were slightly fewer cells on ASTM F1586 in each case but the differences were not significant ($P \geq 0.5$).

In addition, no differences were seen in the rates of attachment, determined by counting the numbers of cells at the four different stages of attachment after 30 min (Fig. 9b). Therefore it was concluded that the high number of cells after just 1 day of incubation is due to the high proliferation rate on the material surface rather than more efficient cell attachment. As it can be seen in Fig. 10, there was no trend in wetability between treated and untreated ASTM F138 and ASTM F1586.

4 Discussion

The biocompatibility of metallic alloys is critical to the success of many implants. In developing new material surfaces for the biomedical industry it is essential that they are screened for corrosion resistance, wear resistance and biocompatibility [19].

Most of the work done in the field of surface modification of biomedical austenitic stainless steel usually focuses on either mechanical or degradation properties rather than biocompatibility [9, 10]. For example, in their paper on plasma immersion ion implantation, PI^3, Mänd et al. [20] relate the effect of degradation (wear or/and corrosion) to biocompatibility without cytotoxicity testing.

Over a span of two decades since the discovery of the S-phase [5] only the papers by Bordji et al. 1996 [15] and Martinesi et al. 2007 [16] mention biocompatibility studies. This has greatly limited the use of S-phase surface engineered medical grade austenitic stainless steel in the biomedical industry.

The results of the biocompatibility tests reported in this work have demonstrated that neither treated nor untreated samples showed any adverse effect on the proliferation of the mouse osteoblast cells used. This contrasts with work by Bordji et al. [15] who observed that cells growing on plasma nitrided samples showed a high degree of cytoincompatibility, which was associated with lower rates of cell proliferation, cell lysis, lower alkaline phosphatase activity and lower levels of osteocalcin production. However it is possible that their results might have been influenced by the presence of iron nitrides on the surface of the S-phase after the nitriding treatment. The removal of the top 1 μm layer from the surface of our samples removed any possibility of superficial contamination.

In the paper by Martinesi et al. [16] the authors compared human umbilical vein epithelial cells and peripheral blood mononuclear cells responses to: untreated, nitrided, and oxidised (nitriding followed by oxidation) stainless steel. Proliferation was slightly diminished and apoptosis increased especially on nitrided followed by oxidation

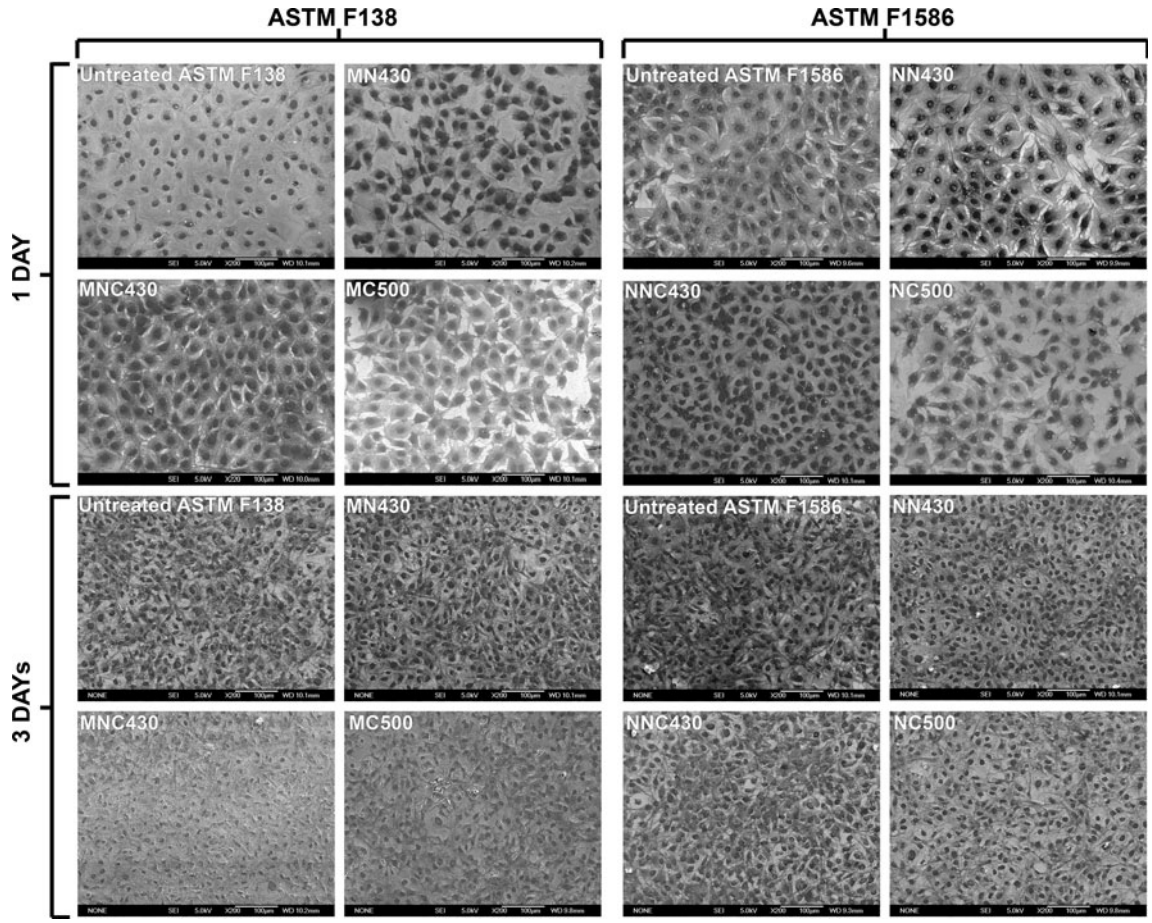

Fig. 6 Scanning Electron Micrographs of MC3T3-E1 Osteoblasts on ASTM F138 (columns 1 and 2) and ASTM F1586 (columns 3 and 4) samples in the untreated and treated form after 1 day (rows 1 and 2) and 3 days (rows 3 and 4) of culture. *Scale Bar* 100 μm

samples. Moreover, on all samples there was a slight increase in production of biological markers associated with inflammation, including the pro-inflammatory cytokines TNF-α and IL-6 and cell adhesion molecules ICAM-1, VCAM-1 and E-selectin. It would be of interest to repeat our experiments with other cell types including epithelial and mononuclear cells and to similarly investigate cytokine and cell adhesion molecule production.

In our experiments it was also noticed that although the osteoblast cells used in the initial cell attachment experiment adhered equally well to all the surfaces tested, there was higher cell proliferation on the treated samples than on the untreated ones (Fig. 5). This might be due to a higher concentration of interstitial elements in the face centred cubic structure of austenitic stainless steel which may be beneficial for osteoblast cell proliferation. The numbers of cells on untreated ASTM F1586 was consistently higher than on untreated ASTM F138, possibly due to higher concentrations of nitrogen in ASTM F1586.

It can be seen in Fig. 3 that the interstitial elements in the nitrided (N430), carburised (C500) and carbonitrided (NC430) layers can reach up to 35 at.% N for S_N, 8 at.% C for S_C and 25 at.% N + 5 at.% C for $S_{C\text{-}N,}$ respectively. The relatively high proliferation of the cells on the $S_{C–N}$ (NC430) samples might suggest that osteoblast cells prefer surfaces that are rich in both nitrogen and carbon. These effects have not previously been reported and merit further investigation with other cell types, testing cell proliferation for longer culture periods and looking for cell differentiation markers.

5 Summary and conclusion

Three types of S-phase layers, S_N, S_C and $S_{C–N,}$ can be formed on medical grade ASTM F138 and F1586 austenitic stainless steel by low temperature plasma surface alloying with nitrogen, carbon and both nitrogen and carbon respectively. Biocompatibility studies on all three S-phase layers, S_N, S_C and $S_{C–N,}$ have indicated, for the first time, that they are biocompatible under the conditions of the tests conducted in this study.

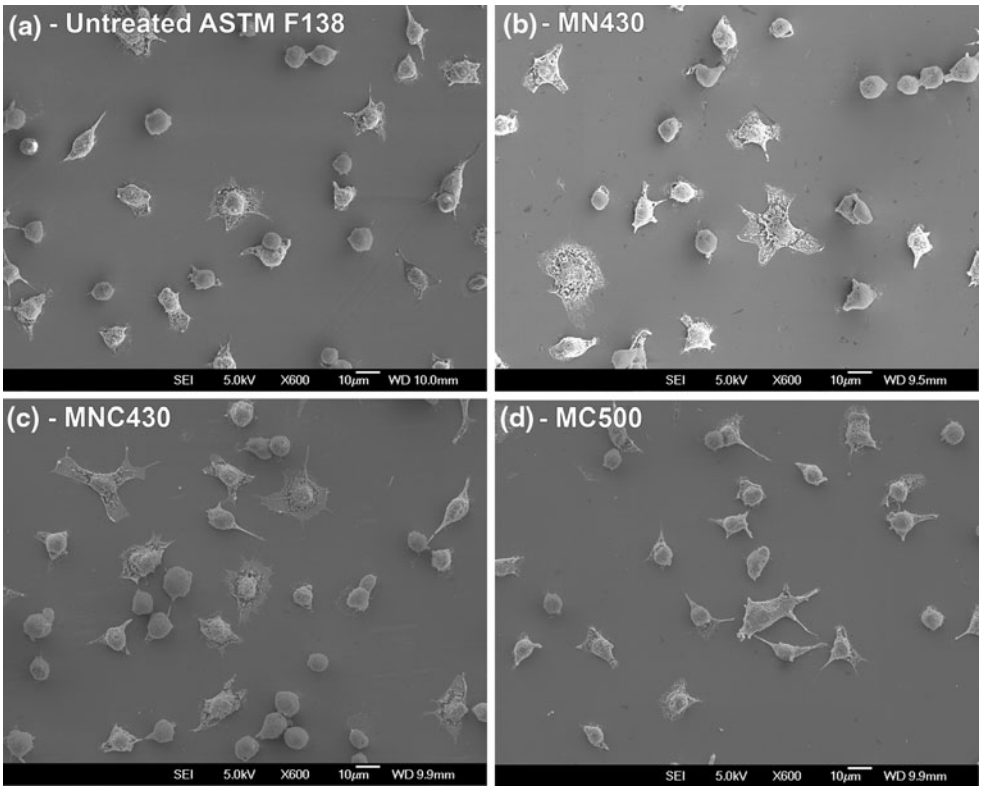

Fig. 7 Scanning Electron Micrographs of initial cell attachment after 30 min incubation on ASTM F138 samples in the **a** untreated; **b** PN at 430°C (MN430); **c** PNC at 430°C (MNC430); and **d** PC at 500°C (MC500) form. *Scale Bar* 10 μm

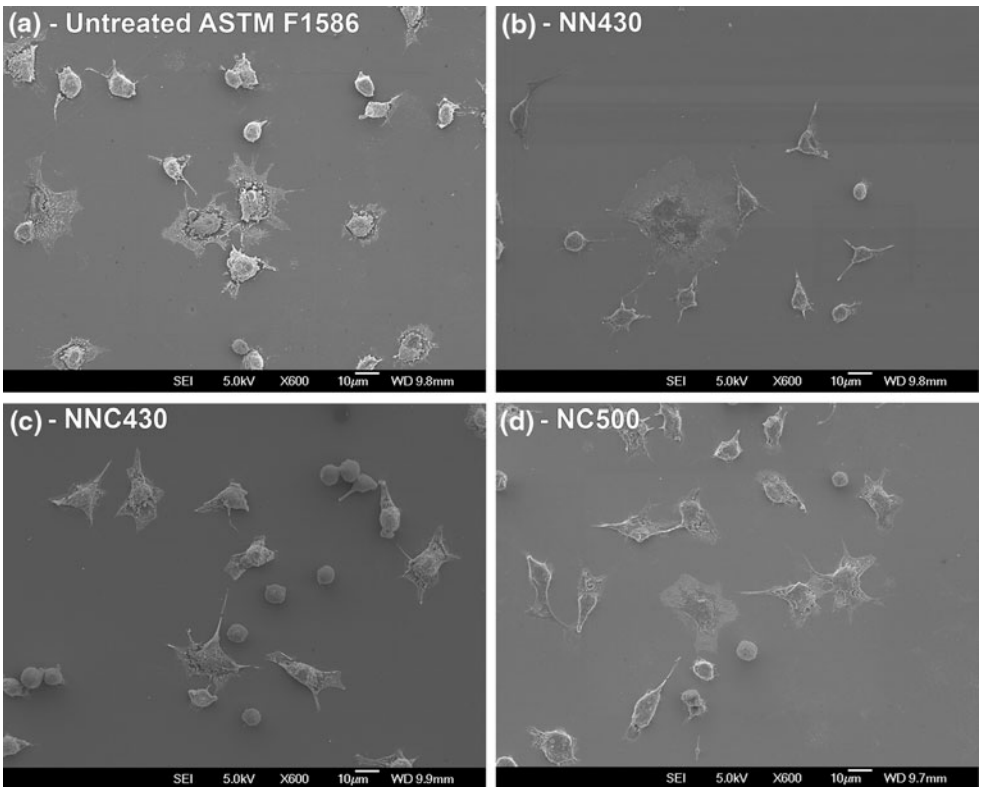

Fig. 8 Scanning Electron Micrographs of initial cell attachment after 30 min incubation on ASTM F1586 samples in the **a** untreated; **b** PN at 430°C (NN430); **c** PNC at 430°C (NNC430); and **d** PC at 500°C (NC500) form. *Scale Bar* 10 μm

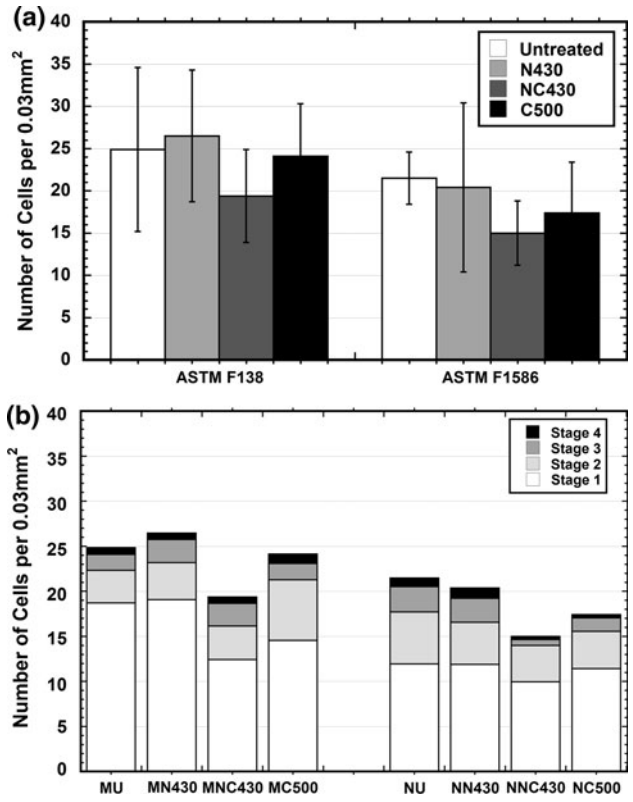

Fig. 9 Cells counted in six random 0.03 mm^2 areas of each disc and classified according to stage of attachment. **a** Total number of cells at all stages (average ± standard deviation); **b** average number of cells at each stage

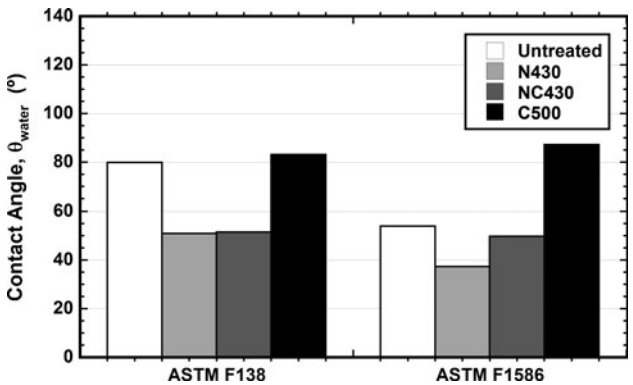

Fig. 10 Contact angle measurements on ASTM F138 and ASTM F1586 (treated and untreated)

The fact that S-phase surface treatment can dramatically increase the hardness and wear resistance of medical grade austenitic stainless steel materials without impairing their corrosion resistance and biocompatibility could pave the way towards high-performance, long-life load-support body implants. The enhanced proliferation of osteoblast cells on the S-phase surfaces could enhance biological fixation of S-phase surface engineered stainless steel implants.

Acknowledgments The authors would like to thank EPSRC, UK for the financial support (EP/C53606/1 and EP/F006926/1). In addition, the authors wish to express their appreciation to their colleagues, Dr. X. Li, Dr. J. Chen, Miss Xin Fu, Miss Anne Jung, Miss Iris Kretzschmar, Miss Yangchun Dong and Mr André Spiteri for their technical support. Dr. J. Buhagiar would like to thank the University of Malta and the University of Birmingham for their financial support.

References

1. Pan J, Karlén C, Ulfvin C. Electrochemical study of resistance of localized corrosion of stainless steels for biomaterial applications. J Electrochem Soc. 2000;147(3):1021–5.
2. Örnhagen C, Nilsson JO, Vannevik H. Characterization of a nitrogen-rich austenitic stainless steel used for osteosynthesis devices. J Biomed Mater Res. 1996;31(1):97–103.
3. Haraldsson C, Cowen S. Characterization of Sandvik Bioline High-N: a comparison of standard grades F1314 and F1586. In: Winters GL, Nutt MJ, editors. Stainless steels for medical and surgical applications. Pittsburg: ASTM International Pittsburg; 2003. p. 3–12.
4. Davis JR, editor. Stainless steels. Ohio: ASM International; 1994.
5. Zhang ZL, Bell T. Structure and corrosion resistance of plasma nitrided stainless steel. Surf Eng. 1985;1(2):131–6.
6. Rolinski E. Effect of plasma nitriding temperatures on surface properties of austenitic stainless steel. Surf Eng. 1987;3(1):35–40.
7. Leyland A, Lewis DB, Stevensom PR, Matthews A. Low temperature plasma diffusion treatment of stainless steels for improved wear resistance. Surf Coat Technol. 1993;62(1–3):608–17.
8. Blawert C, Mordike BL, Collins GA, Short KT, Jiraskova Y, Schneeweiss O, et al. Characterisation of duplex layer structures produced by simultaneous implantation of nitrogen and carbon into austenitic stainless steel X5CrNi189. Surf Coat Technol. 2000;128–129:219–25.
9. Saklakoglu N, Saklakoglu IE, Short KT, Collins GA. Tribological behavior of PIII treated AISI 316 L austenitic stainless steel against UHMWPE counterface. Wear. 2006;261(3–4):264–8.
10. Lei MK, Zhu XM. In vitro corrosion resistance of plasma source ion nitrided austenitic stainless steels. Biomaterials. 2001;22(7):641–7.
11. Rayner B, Li XY, Dong H. Preliminary study on plasma surface modification of medical grade 316LVM and high nitrogen austenitic stainless steels. Surf Eng. 2006;22(2):103–8.
12. Buhagiar JP, Dong H. Low-temperature plasma surface modification of medical grade austenitic stainless steel to combat wear and corrosion. Key Eng Mater. 2008;373–374:296–9.
13. Buhagiar J, Dong H, Bell T. Low temperature plasma surface alloying of medical grade austenitic stainless steel with C & N. Surf Eng. 2007;23(4):313–7.
14. Dong H. S-phase surface engineering of Fe–Cr, Co–Cr and Ni–Cr alloys. Int Mater Rev. 2010;55:65–98.
15. Bordji K, Jouzeau J-Y, Mainard D, Payan E, Delagoutte J-P, Netter P. Evaluation of the effect of three surface treatments on the biocompatability of 316L stainless steel using human differentiated cells. Biomaterials. 1996;17(5):491–500.
16. Martinesi M, Bruni S, Stio M, Treves C, Bacci T, Borgioli F. Biocompatibility evaluation of surface-treated AISI 316L austenitic stainless steel in human cell cultures. J Biomed Mater Res A. 2007;80(1):131–45.

17. Li XY, Buhagiar J, Dong H. Characterisation of dual S phase layer on plasma carbonitrided biomedical austenitic stainless steels. Surf Eng. 2010;26(7):67–73.
18. Rajaraman R, Rounds DE, Yen SP, Rembaum A. A scanning electron microscope study of cell adhesion and spreading in vitro. Exp Cell Res. 1974;88:327–39.
19. Bailey LO, Lippiatt S, Biancanello FS, Ridder SD, Washburn NR. The quantification of cellular viability and inflammatory response to stainless steel alloys. Biomaterials. 2005;26(26): 5296–302.
20. Mändl S, Rauschenbach B. Improving the biocompatibility of medical implants with plasma immersion ion implantation. Surf Coat Technol. 2002;156(1–3):276–83.